Asia-Pacific J. Atmos. Sci., 49(5), 571-586, 2013
DOI:10.1007/s13143-013-0051-9

Numerical Simulations of Asian Dust Events: A Lagrangian Dust Model and Its Applications

Cheol-Hee Kim and Hyo-Jung Lee

Department of Atmospheric Sciences, Pusan National University, Busan, Korea

(Manuscript received 13 October 2012; revised 25 March 2013; accepted 25 March 2013)
© The Korean Meteorological Society and Springer 2013

Abstract: An uni-modal Lagrangian Dust Model (LDM) was developed to simulate the dust concentrations and source-receptor (S-R) relationships for recent Asian dust events that occurred over the Korean Peninsula. The following dust sources were used for the S-R calculation in this study: S-I) Gurbantunggut desert, S-II) Taklamakan desert, S-III) Tibetan Plateau, S-IV) Mu Us Desert, S-V) Manchuria, and S-VI) Nei Mongol and Gobi Desert. The following two 8-day dust simulation periods were selected for two case studies: (Period A) March 15-22, 2011, and (Period B) April 27-May 4, 2011. During two periods there were highly dense dust onsets observed over a wide area in Korea. Meteorological fields were generated using the WRF (Weather Research and Forecasting) meteorological model, and Lagrangian turbulent properties and dust emission were estimated using FLEXPART model and ADAM2 (Asian Dust Aerosol Model 2), respectively. The simulated dust concentrations are compared with point measurements and Eulerian model outputs. Statistical techniques were also employed to determine the accuracy and uncertainty associated with the model results. The results showed that the LDM compared favorably well with observations for some sites; however, for most sites the model overestimated the observations. Analysis of S-R relationships showed that 38-50% of dust particles originated from Nei Mongol and the Gobi Desert, and 16-25% of dust particles originated from Manchuria, accounting for most of the dust particles in Korea. Because there is no nudging or other artificial forcing included in the LDM, higher error indicators (e.g., root mean square error, absolute gross error) were found for some sites. However, the LDM was able to satisfactorily simulate the maximum timing and starting time of dust events for most sites. Compared with the Eulerian model, ADAM2, the results of LDM found pattern correlations (PCs) equal to 0.78-0.83 and indices of agreement (IOAs) greater than 0.6, suggesting that LDM is capable of estimation of dust concentrations with the quantitative information on the S-R relationships that can be easily obtained by LDM.

Key words: Asian dust simulations, Lagrangian Dust Model (LDM), source-receptor relationship

1. Introduction

Major sources of Asian dust are arid and/or semi-arid regions, such as the Taklamakan desert, Gobi desert, and Loess plateau in China and Mongolia. Dust can be uplifted into the atmosphere by the strong surface winds (particularly during spring season) in the source regions, causing respiratory and eye disease, and resulting in changes in the chemical composition of soil (Hagen and Woodruff, 1973). In addition, dust can cause cattle suffocation, visibility reduction leading to airport closures and road accidents (Buritt and Hyers,1981), damage to sensitive scientific and industrial equipment, and corrosion of buildings and monuments (Goudie, 1977). Recently, there is an increasing interest in mineral dust because of its significant impact on global climate change and global air quality. Mineral dust also plays an important role in altering the earth's radiative budget through the scattering and absorption of solar radiation (Haywood and Boucher, 2000; Harrison *et al.*, 2001).

Models of dust emission and transport play an important role in forecasting and understanding dust distribution. In East Asia, studies of Asian dust focus on both the source regions and transport processes to improve dust prediction. Previous modeling studies showed that the models have reproduced many important observational facts and retrieved valuable information to elucidate characteristics of Asian dust phenomena (Wang *et al*., 2000; Gong *et al*., 2003; Liu *et al*., 2003; Park and In, 2003; Shao *et al*., 2003; Uno *et al*., 2001, 2003). In Korea, after an extraordinarily severe Asian dust event was observed for the years of 2001-2002, the three-dimensional Eulerian dust forecasting model named Asian Dust Aerosol Model (ADAM) was developed by the Meteorological Administration to forecast the Asian dust storm events (In and Park, 2003; Park and Lee, 2004). Later, Asian Dust Aerosol Model ver. 2 (ADAM2), which extended the model domain of ADAM, was developed to predict Asian dust with the observed meteorological data obtained from towers in the source regions (Park and In, 2003; Park and Lee, 2004).

Like other air pollution models, dust transport modeling can be carried out in either Eulerian or Lagrangian frames. Eulerian dust transport and diffusion solutions are achieved over the fixed grids where the fundamental advective tendency equation is explicitly solved. However, it is known that existing Eulerian transport algorithms sometimes contain appreciable errors, known as numerical diffusion, and spurious oscillations that are a result of calculating features that are not resolved by more than several grid cells (Chock and Winkler, 1994; Dabdub and Seinfeld, 1994; Collins *et al*., 1997; Russell and Dennis, 2000; Song *et al*., 2003). Because of these errors, the Lagrangian

Corresponding Author: Cheol-Hee Kim, Department of Atmospheric Sciences, Pusan National University, San 30, Jangjeon-Dong, Geumjeong-Gu, Busan 609-735, Korea.
E-mail: chkim2@pusan.ac.kr

approach is more advantageous than the Eulerian one. The Lagrangian method can avoid the computational complexities associated with finding simultaneous solutions of many differential equations, and can obtain relatively good performance in assessing medium- or long-range transport (Peters *et al*., 1995; Stohl, 1998). In the Lagrangian frame, the source-receptor (S-R) relationship can be easily obtained by relatively simple performance without heavy computational cost.

In this study, we introduce a Lagrangian Dust Model (LDM) that was developed for the simulations of Asian dust in a Lagrangian frame. The LDM is applied to the recent Asian dust events. The simulations of dusts for the two selected periods are continuously integrated without nudging or restarting the simulations. A comparison of the LDM results was made against the Eulerian model ADAM2 outputs and the observation data. The effectiveness of the Lagrangian approach in simulating dust concentrations without any artificial nudging or forcing was evaluated and discussed comparatively. It is also examines the use of LDM to determine S-R relationship calculations. In order to derive S-R relationships, six Asian dust source regions are identified and multiple source-receptor matrices are derived to discuss the source-related dust particles.

2. Methodology

In order to integrate the dust trajectory equation, Lagrangian transport process generally uses the following simple first order scheme,

$$X(t + \Delta t) = X(t) + v(X, t)\Delta t,$$

where X is the position vector; t, time; Δt, the time increment; and $v = \bar{v} + v_t$, the wind vector that is composed of the grid scale wind $\bar{v}$ and the turbulent wind fluctuations v_t. Turbulent motions v_t for each wind component i are parameterized assuming a Markov process based on the following Langevin equation (Thomson, 1987):

$$dv_{ti} = a_i(x, v_t, t)dt + b_{ij}(x, v_t, t)dW_j,$$

where the drift term a and the diffusion term b are functions of position, turbulent velocity, and time, and dW_j are incremental components (uncorrelated with time) of a Wiener process with mean zero and variance dt (Legg and Raupach, 1982). For model development of LDM in this study, the FLEXPART model was selected to modulate the Langevin equation. The turbulent properties considered in this LDM are described in Appendix A.

Dust concentration in a grid cell is calculated by a simple uniform kernel method that is based on sampling the tracer mass fractions of all particles within the grid cell and dividing by the grid cell volume,

$$C(x, y, z) = \frac{1}{V}\sum_{i=1}^{i=N}(m_i \cdot f_i)$$

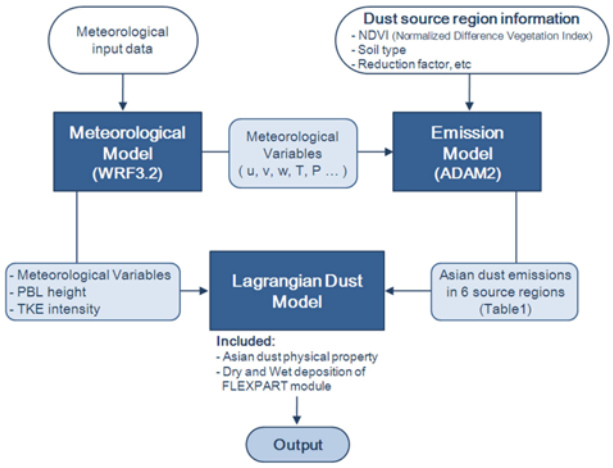


Fig. 1. Flow chart of the Lagrangian Dust Model (LDM) for simulating Asian dust.

where V is the grid cell volume, m_i, particle mass, N, the total number of particles, and f_i, the fraction of the mass of particle i attributed to the respective grid cell. This mass fraction is calculated by a uniform kernel estimator with bandwidths (Δx, Δy), where Δx and Δy are the grid distances on the longitude-latitude output grid.

LDM has been developed by coupling three modules: meteorological model WRF, Lagrangian transport module in FLEXPART, and dust emission module of ADAM2. Figure 1 illustrates a flowchart of model development of LDM for experimental design in this study. The FLEXPART module is employed to calculate Lagrangian transport process in LDM because it has many capabilities including forward dispersion calculation, backward response functions, trajectory cluster calculation, removal processes, uncertainty calculation, age spectra calculation, and mass flux calculation; in addition, the model is well documented through the studies. FLEXPART model is designed to perform particle dispersion computations based on wind fields derived from the ECMWF global forecast model. The full description of the model is given in Stohl *et al*. (2005). However, FLEXPART model is not compatible with both the WRF meteorological model and dust emission module of ADAM2. Thus, we have coupled FLEXPART model with dust emission module by modifications of the two models for the model compatibility, as illustrated in Fig. 1.

a. Analysis regions and simulation cases

The domain of current study is shown in Fig. 2. We subdivided dust source regions into six analysis regions according to previous studies (Kurosaki and Mikami, 2003, 2005; Lim and Chun, 2006). The six source regions are: S-I) the Gurbantunggut Desert, S-II) the Taklamakan Desert, S-III) the Tibetan Plateau, S-IV) the Mu Us Desert, S-V) Manchuria, and S-VI) Nei Mongol and the Gobi Desert. We labeled the six source regions S-I through S-VI, as indicated in Fig. 2. Table 1 summarizes the characteristics of the six dust source regions.

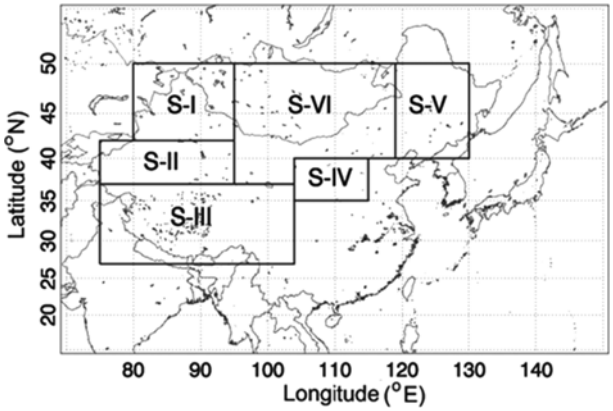


Fig. 2. Subdivided Asian dust source regions used in this study.

The Gurbantunggut (S-I) and the Taklamakan Desert (S-II) are located in the Tarim Basin, surrounded by high mountains comprising the Tibetan Plateau, Pamirs, and the Tian Shan Mountains. The elevation of two source regions (S-I and S-II) are both more than 2,000 m above sea level. The area of Nei Mongol and the Gobi Desert (S-VI) shows the largest in area among six regions as indicated in Fig. 2. The Gobi Desert extends from the south of Mongolia to the north of China, and its major land cover type is semi-desert shrubs. The land cover type of Nei Mongol is grassland and the region's climate is well characterized by a low annual precipitation of about 100 mm and the prevailing northwesterlies. In the Gobi desert area (S-VI), the annual frequency of strong wind speeds exceeding 15 m s^{-1} is more than 20% and the annual number of dust storm days is more than 50 days (Batsukh, 2004; Kurosaki and Mikami, 2007). In source regions S-II, S-IV, and S-V, the major land-cover types are semi-desert shrubs in the western part, cultivated land in the southeastern part, and grassland in the northeastern part. The details of soil types over the six source regions are listed in Table 1.

For the performance test of LDM simulations, two cases with major 8-day (192 hours) dust episodes were selected: (Period A) March 15-22, 2011 and (Period B) April 27-May 4, 2011. During Period A, very dense dust onsets were observed over a wide area, including China and Korea. The observed maximum PM_{10} concentration exceeded 1,500 μg m^{-3} in Beijing and 1,300 μg m^{-3} in Seoul, on March 19, 2011. Over Period B, the maximum PM_{10} concentration exceeded 790 μg m^{-3} in Seoul on May 1, 2011. For both Periods A and B, the Eulerian model ADAM2 was also used to simulate a quantitative comparison against the LDM simulations.

b. Model and experimental setup

The meteorological model coupled here in LDM model is the Weather Research and Forecasting (WRF) model (Klemp *et al*., 2000) which is a next-generation mesoscale meteorological forecast model developed by a collaboration of many research groups. The equation sets of the WRF model are the non-hydrostatic primitive equations, including momentum, thermodynamics, and moisture, with physical processes for convective parameterization, the mixed-phase scheme, the planetary boundary layer processes, and the radiation transfer processes.

Since the WRF model is relatively new, we developed the LDM to make it compatible with the WRF model so the multi-scale meteorological predictions made by the WRF model can be used to forecast Asian dust concentrations and analyze S-R relationships. The meteorological model, WRF, in this case study, is run using 27 vertical layers, with 340 × 230 horizontal grids with a resolution of 30 km. As a microphysics options, WSM 6-class graupel scheme as microphysics, rrtm scheme and Dudhia scheme as long and short wave radiation schemes are used, respectively. Other details including model options and WRF configurations employed in this study are summarized in Table 2.

LDM employed Lagrangian transport module of FLEXPART, to calculate transport process by mean and turbulent fluctuations. In FLEXPART model, parameterization schemes based on the boundary layer parameters such as surface layer height, roughness length, Monin-Obukhov length scale, friction velocity,

Table 1. Locations of Asian dust source regions used in this study.

#	Desert	Locations	Soil Type (%)				Remarks
			Gobi	Sand	Loess	Mixed	
S-I	Gurbantunggut Desert	80-95°E, 42-50°N	11.3	11.7	2.5	31.8	Yang and Ding (2008), Wang *et al*. (2009), Xu *et al*. (2009)
S-II	Taklamakan Desert	75-95°E, 37-42°N	12.9	33.3	0.2	48.3	Yang and Ding (2008), Wang *et al*. (2009), Xu *et al*. (2009)
S-III	Tibetan Plateau	75-104°E, 27-37°N	-	0.9	1.0	47.9	Park and Lee (2004)
S-IV	Mu Us Desert	104-115°E, 35-40°N	-	14.0	47.3	25.2	Yang and Ding (2008), Wang *et al*. (2009), Xu *et al*. (2009)
S-V	Manchuria	119-130°E, 40-50°N	-	6.3	14.5	26.4	Chun *et al*. (2003), Xu *et al*. (2009), Kurosaki and Mikami (2005), Kim *et al*. (2010)
S-VI	Nei Mongol and Gobi Desert	95-119°E, 37(40)-50°N	22.5	8.6	12.5	42.2	In and Park (2003)

Table 2. Model configurations and options selected in WRF meteorological model.

WRF microphysics and model configurations	Selection of schemes and configurations
Microphysics scheme	WRF 6-class graupel scheme
Boundary layer scheme	YSU scheme
Cumulus parameterization scheme	Kain-Fritsch scheme
Surface layer scheme	Monin-Obukhov similarity theory
Land-surface scheme	Noah Land Surface Model
Long-wave radiation scheme	RRTM scheme
Short-wave radiation scheme	Dudhia scheme
Horizontal grids	340 × 230
Horizontal spacing (km)	30 km
Vertical layers	27 layers

convective velocity scale, and convective boundary layer height are used (Ryall *et al*., 1997; Hanna, 1982). FLEXPART takes into account both wet and dry depositions by reducing a particle's mass. In wet deposition process, in-cloud and below-cloud scavenging were treated separately (Asman, 1995), and the deposition velocity of a gas is calculated with the resistance method (Wesely and Hicks, 1977). The details of turbulent properties in LDM are described in Appendix A, and the wet and dry removal processes derived from the FLEXPART module (Stohl *et al*., 2005) is summarized in Appendix B.

c. Dust emission

One of the largest uncertainties in Asian dust simulation is the emission strength in various source regions. Generally, it is known that dust mobilization is initiated when a strong wind blows over dry and sparse vegetation areas. Because of this, many studies have parameterized the uplifting process using the wind speed, soil water content, and vegetation cover (Tegen and Fung, 1994).

In this study, we employed an emission module of ADAM2 for running LDM (Fig. 1), which was developed using a time series of the WMO synoptic reporting data for the entire East Asian domain (In and Park, 2002; Park and In, 2003). In and Park (2002) studied a large number of locations of WMO synoptic stations over East Asia and reported and analyzed the weather codes at these stations to identify the locations and frequencies of dust rises for delineating the dust source regions. In previous studies, the statistical threshold wind speeds for dust-rise condition estimated by ADAM2, are 9.5, 7.5, 6.0, and 9.2 m s^{-1} at 10 m above the ground level in the Gobi, sand, Loess, and Mixed soil regions, respectively. More details are found in Park and In (2003) and In and Park (2003).

4. Results

a. Meteorological fields

Figure 3 shows the simulated horizontal distributions of 850 hPa pressure fields with wind vectors at 0000UTC for Periods A and B, and Fig. 4 indicates 850 hPa weather maps provided by Korean Meteorological Administration for the same two periods. For both periods, the location of the anticyclone played an important role in dust mobilization over the source regions and transport processes toward Korean Peninsula. For Period A, on March 15, a strong anticyclone pressure is seen over mainland western China at around 110°E longitude and 38°N latitude at 0000 UTC, and it steadily moved eastward (Figs. 3 and 4). This continental anticyclone extended over central China and significantly affected wind direction and the transport of Asian dust. On March 17, a low-pressure system located in northwest China emerged at 115°E longitude and 55°N latitude and caused strong pressure gradients, with a result of it being located close to the high pressure system in the southwestern China (Figs. 3 and 4). This resulted in strong northwesterlies

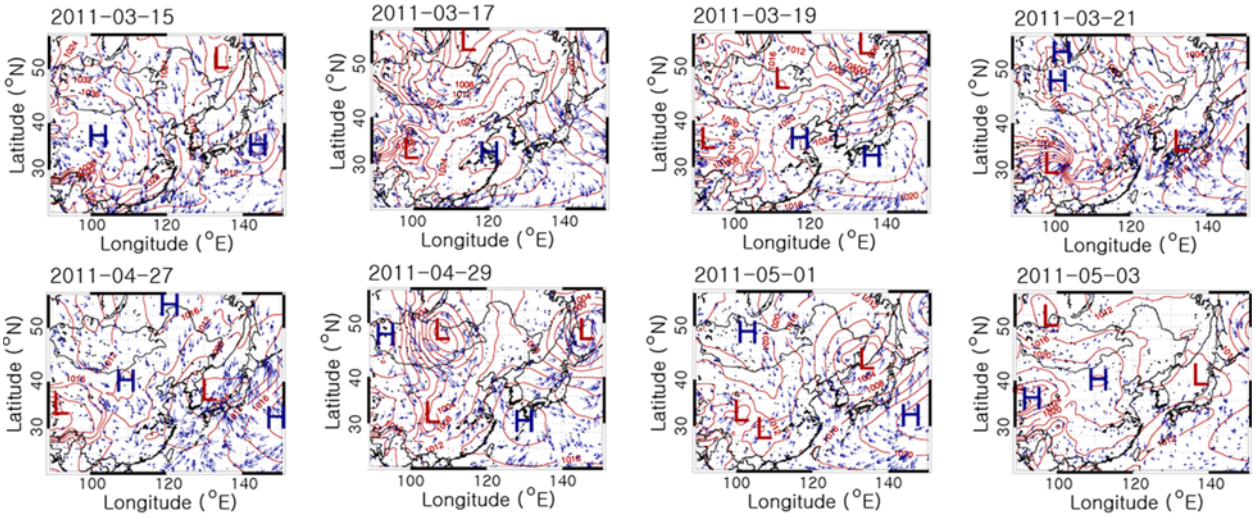


Fig. 3. Simulated 850 hPa synoptic weather patterns on March 15, 17, 19, and 21, 2011, during Period A (top panel) and April 27, 29, May 1, and 3, 2011, during Period B (bottom panel).

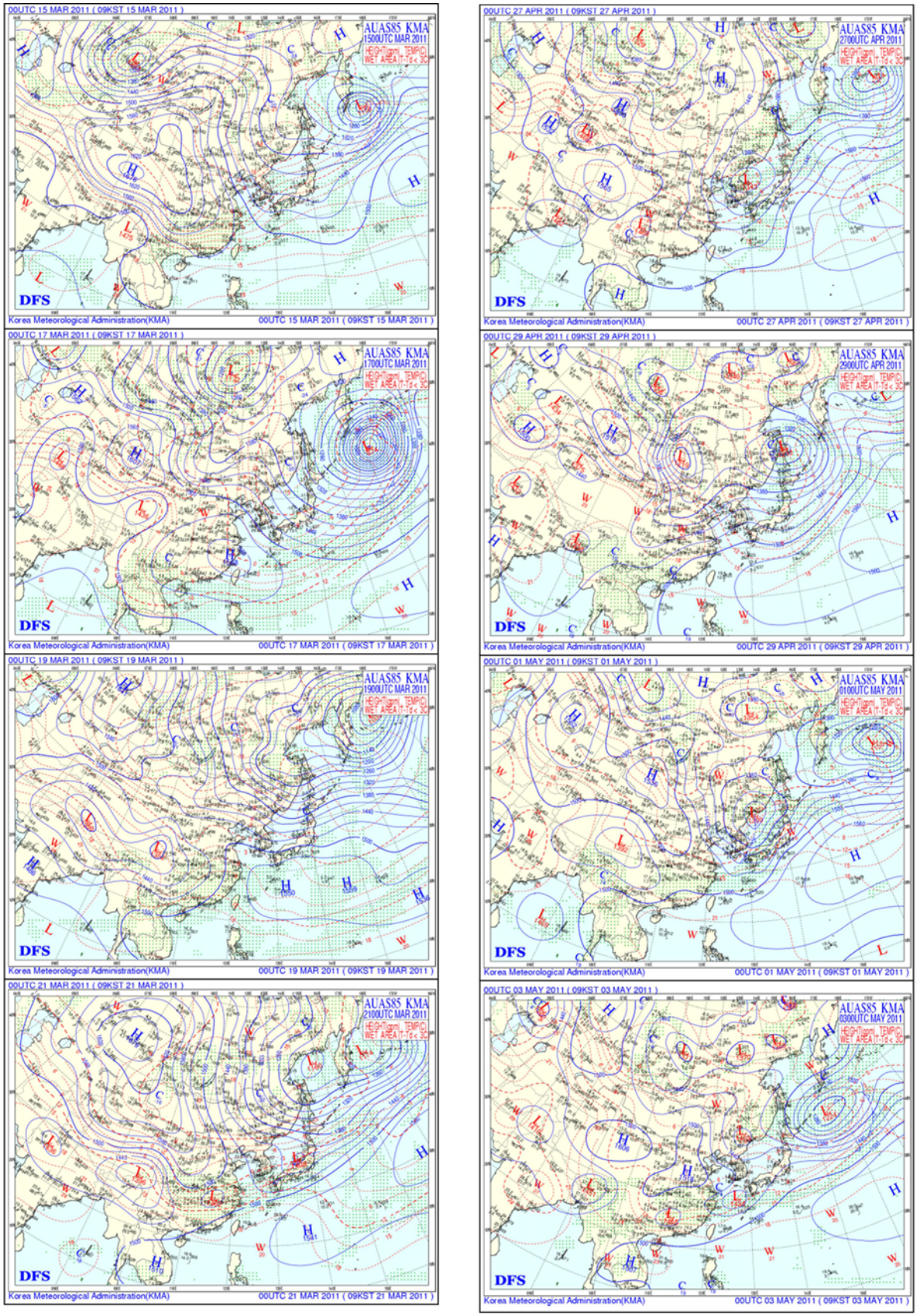


Fig. 4. 850 hPa synoptic weather maps on March 15, 17, 19, and 21, 2011, during Period A (left panel) and April 27, 29, May 1, and 3, 2011, during Period B (right panel), provided by KMA (Korean Meteorological Administration).

over the dust source regions of S-I and S-VI. This pressure system maintained a pressure gradient force that served the westerly and northwesterly winds from eastern China to western Korea, which was conducive to long-range transport of Asian dust toward the Korea peninsula.

On March 19, the low-pressure system elongated through central China at 0000 UTC and the high-pressure system was located over the area between southeastern Korea and south Japan at 0000 UTC. These locations caused southeasterlies over the Korean Peninsula (Fig. 3). On March 20, the trough had passed over Korean Peninsula.

For period B, on April 29-30, the low-pressure system formed at 110°E longitude and 50°N latitude, and cause significantly strong northwesterlies over the dust source regions S-VI and S-IV. On April 29-May 1, a high-pressure system located near the southern area of the Korean Peninsula showed conditions similar to that of March 17 in Period A (Figs. 3 and 4). This meteorological system maintained until May 1, consistently generating southeasterlies over the Korean Peninsula. After May 1, this cyclone system passed through the north of Korean Peninsula, followed by a migratory high pressure emerged over northwest China.

Overall, the pressure patterns were well simulated in terms of locations of pressure system and wind patterns, only with some exceptions over the limited area of southwest China. The analysis of synoptic weather charts matched well with the model simulations, particularly in northwest China and eastern Japan (see Figs. 3 and 4).

b. Dust emission

Figure 5 shows the spatial distributions of 8-day (192 hours) accumulated dust emission distributions estimated by ADAM2 over a 30 km × 30 km horizontal grid scale over two periods. The majority of dust emissions for Periods A and B was contributed by the source region S-VI, which occupies more than 30% of the six total source areas indicated in Fig. 2. Table 3 shows the estimated dust emission over the six source regions. As listed in Table 3, the total accumulated dust emission is estimated to be about 1.52×10^8 ton in the whole source regions for Period A. Of the six source regions, S-VI (Nei Mongol and the Gobi Desert) has the largest area of dust rise. A total of 44.6% of dust (6.81×10^6 ton) is contributed by S-VI during Period A, by far the largest fraction of dust in this period. The next largest contribution is 14.4%, originating form S-III. The source regions S-IV, S-V, and S-I contributed 13.2% (2.02×10^6 ton), 10.3% (1.58×10^6 ton), and 6.0% (9.22×10^5 ton), respectively.

Period B also shows no significant difference in comparison with Period A. The total accumulated dust emission estimated by the model is about 3.43×10^7 ton over Period B. Of the six dust source regions, 1.64×10^7 ton (47.9%) is contributed by S-VI, the same region that contributed the largest fraction during Period A. The second largest contribution is made by S-III, which contributed 12.9% of the total dust. The source regions

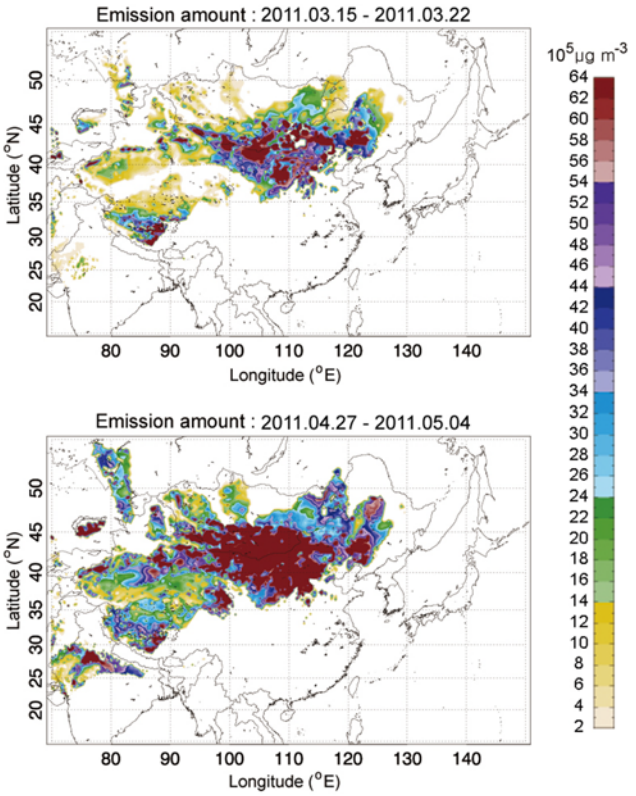


Fig. 5. Emission amounts of Asian dust for a) Period A (March 15-22, 2011) and b) Period B (April 27-May 4, 2011).

Table 3. Simulated dust emission in each of the source regions estimated by ADAM2 for Periods A and B.

Total Dust Emissions (ton)	Period A	Period B
S-I	922,089.3 (6.0%)	2153,243.3 (6.3%)
S-II	892,457.6 (5.8%)	2884,497.0 (8.4%)
S-III	2193,835.8 (14.4%)	4425,961.0 (12.9%)
S-IV	2017,845.8 (13.2%)	3063,306.3 (8.9%)
S-V	1575,384.5 (10.3%)	2257,098.5 (6.6%)
S-VI	6810,633.5 (44.6%)	16420,336.0 (47.9%)
Others	860,828.2 (5.6%)	3096,646.0 (9.0%)
Total	15,273,074.6 (100%)	34,301,088.0 (100%)

S-IV, S-II, and S-V contributed 8.9% (3.06×10^6 ton), 8.4% (2.88×10^6 ton), and 6.6% (2.26×10^5 ton), respectively. The estimated dust-rise regions coincided well with the areas where strong wind speed occurred, as indicated in Fig. 3, particularly on March 15.

The temporal variation in the dust emission in each source region indicates that the largest hourly total dust emission with highly strong time variations occurred in Nei Monglo and the Gobi desert. These regions had larger emission areas and stronger wind speeds than the other source regions (not shown here). Previous studies found that the model underestimated the friction velocity, particularly in the Loess region (In and Park,

2003). This may cause smaller dust estimation in the regions with a large dust-rise area (e.g., S-IV in this study). However, in other regions such as mixed and sand regions, friction velocity estimated by the model is comparable with observations in magnitude (In and Park, 2003). This is believed to yield a relatively lower bias of the dust emission.

c. Spatial distributions of dust concentration

Figure 6 shows spatial distributions of dust particles for the two periods. Each of the six dust colors indicates its source: S-I (brown), S-II (orange), S-III (yellow), S-IV (green), S-V (blue), and S-VI (purple). On March 16, a large amount of dusts originated from S-VI, was transported to central China and then moved toward southeastern China (Fig. 6). This transport process is directly due to the northeasterly wind over the inland region of China, as outlined in Figs. 3 and 4. Over the Korean Peninsula, on March 15-16, dust emitted from source region S-VI merged with dust from S-V, and a large number of particles from either S-VI or S-V were found in Korea (Fig. 6).

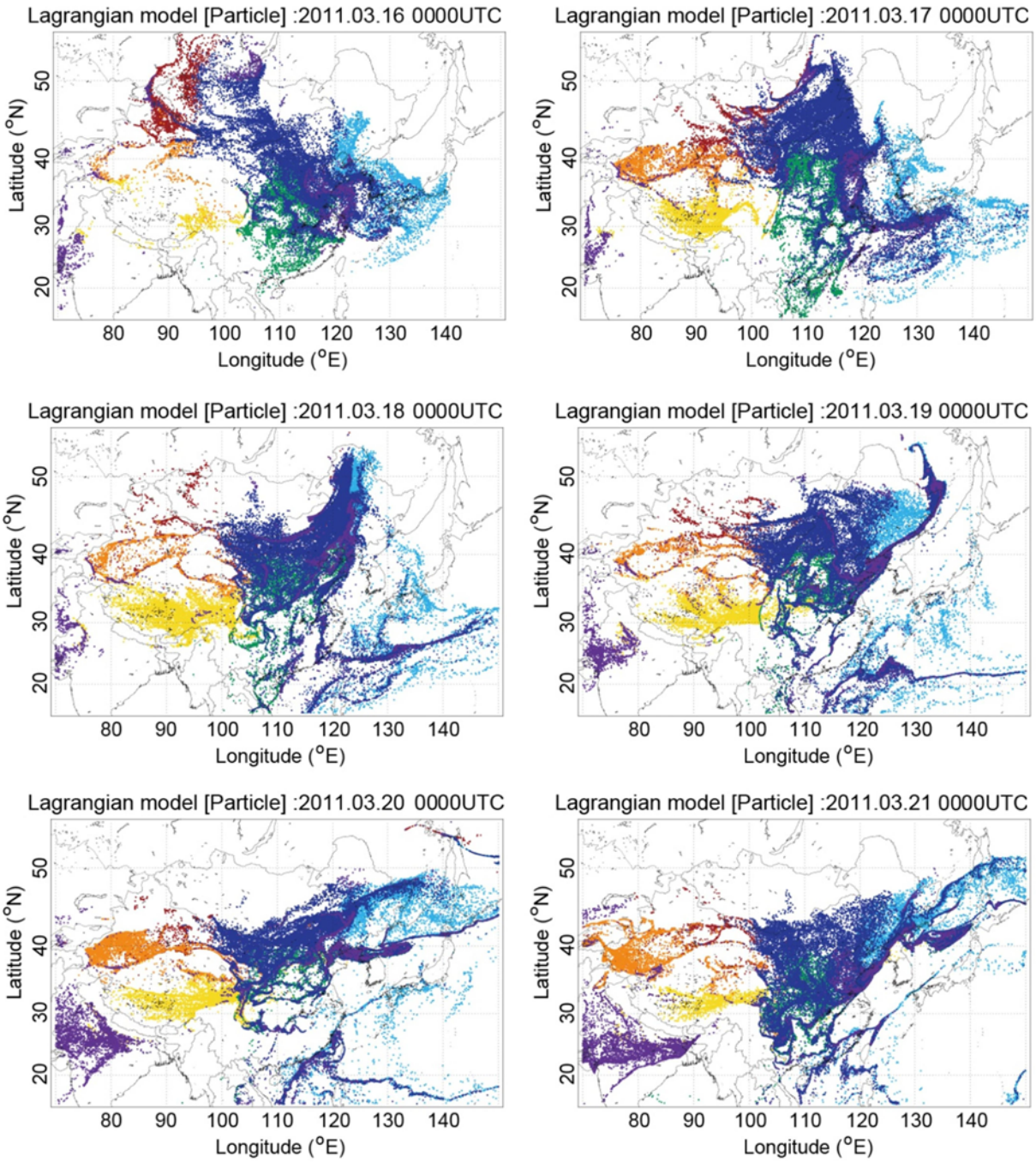


Fig. 6. Spatial distributions of the simulated Lagrangian particles for Period A.

On March 17, the dust-laden air moved continuously southward or southeastward, and a large number of dust particles originating from S-VI were located over the southern ocean of Korean. On March 19, a high-pressure system located over the Korean Peninsula (Figs. 3 and 4) transported dusts continuously northeastward over the Korean Peninsula (Figs. 4 and 6). The progression of the meteorological field controlled the movement of the dust layer after March 16, and the dust-laden air in both eastern China and the Korean Peninsula moved clockwise in association with the high-pressure system. As a result, dust mostly approached northeast China and Manchuria after March 19, 2011. In addition, on March 19, 2011, southwestlies prevailed over the Korean Peninsula and propelled dust-laden air over the Korean Peninsula in the northeast direction, blocking subsequent dust transport from the major source regions.

Over Period B, the pattern of high concentration in Fig. 7 correlated strongly with the strong wind speed regions shown in Fig. 3. Overall, the horizontal pattern resembled that for Period A, as indicated in Fig. 6. However, there are some differences in particle origin. On April 28-29, dust particles originating from S-V mainly affect the Korean Peninsula because of the wind patterns caused by the high-pressure

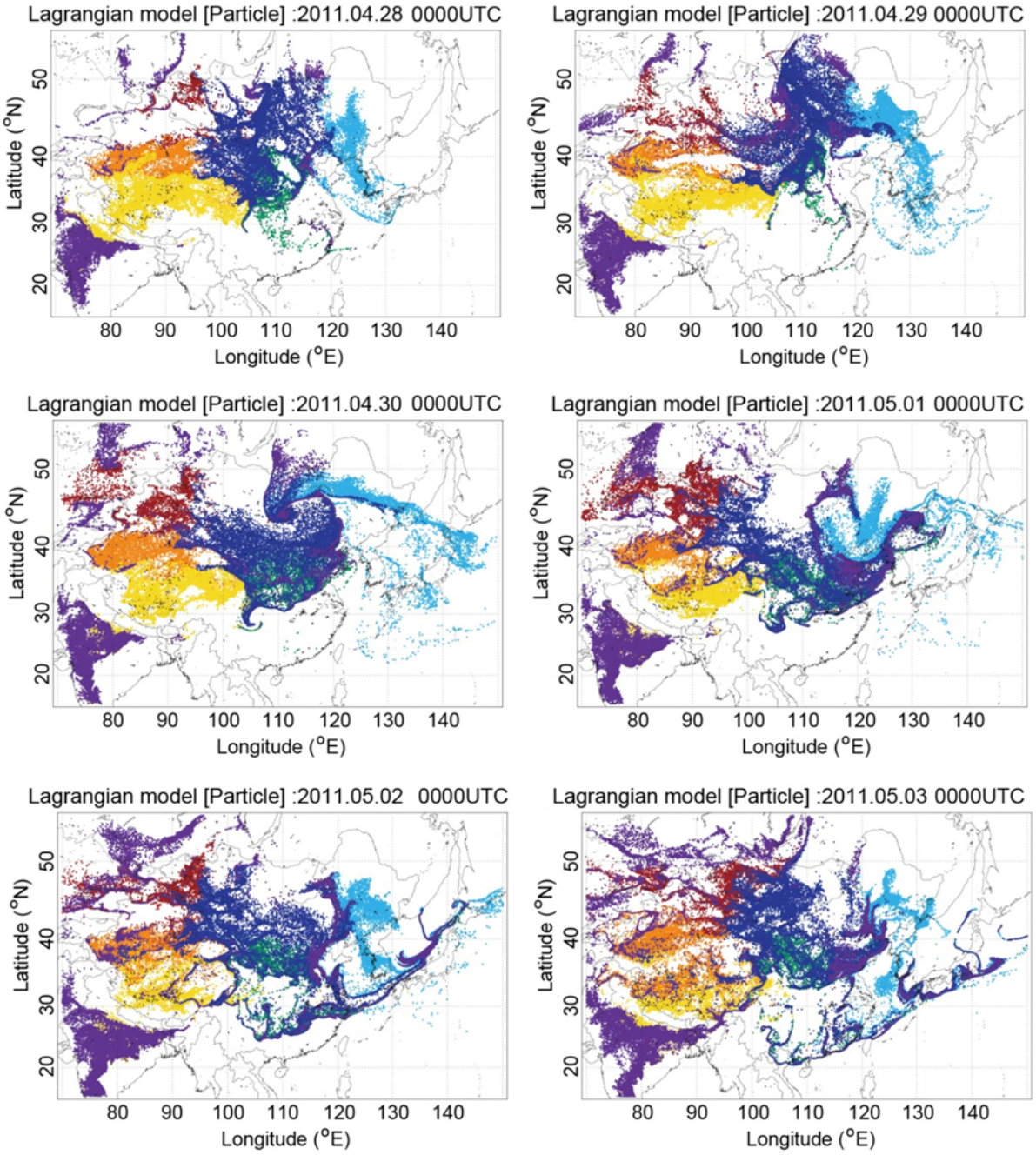


Fig. 7. Spatial distributions of the simulated Lagrangian particles for Period B.

system located in northeastern China described above (Fig. 3). However, dust originating from S-VI had a smaller effect on the Korean Peninsula during Period because of the location where the cyclone induced southwesterlies over the South Sea. During the period April 29-May 1, southerlies caused by an anticyclone over the South Sea governed particle transport near the Korean Peninsula, resulting in an additional significant dust transport toward the western area of Korean Peninsula (Fig. 6). On May 2, some transportation of dust from the southern China through the southern ocean near the Korean Peninsula was simulated.

d. Comparison against observation sites

Figures 8-9 show a comparison of the simulated dust concentrations against hourly measurements of PM_{10} concentrations at eight sites (two sites × four metropolitan cities; Seoul, Gwangju, Busan, and Daegu) during each period. These figures show the S-R relationships denoted with different colors for the six source regions: S-I (brown), S-II (orange), S-III (yellow), S-IV (green), S-V (light blue), S-VI (dark blue), and others (purple). It should be also noted that the simulated concentrations were taken as the simulated mean grid values estimated using the uniform kernel method described in Chapter 2.1. However, the locations of the corresponding monitoring sites are all point values.

During Period A, strong peaks were observed on March 19 at both the Seoul and Mt. Gwanak sites. The Seoul and Mt. Gwanak sites showed the highest dust concentrations with peaks of more than 600 μg m^{-3}. The simulated maximum value

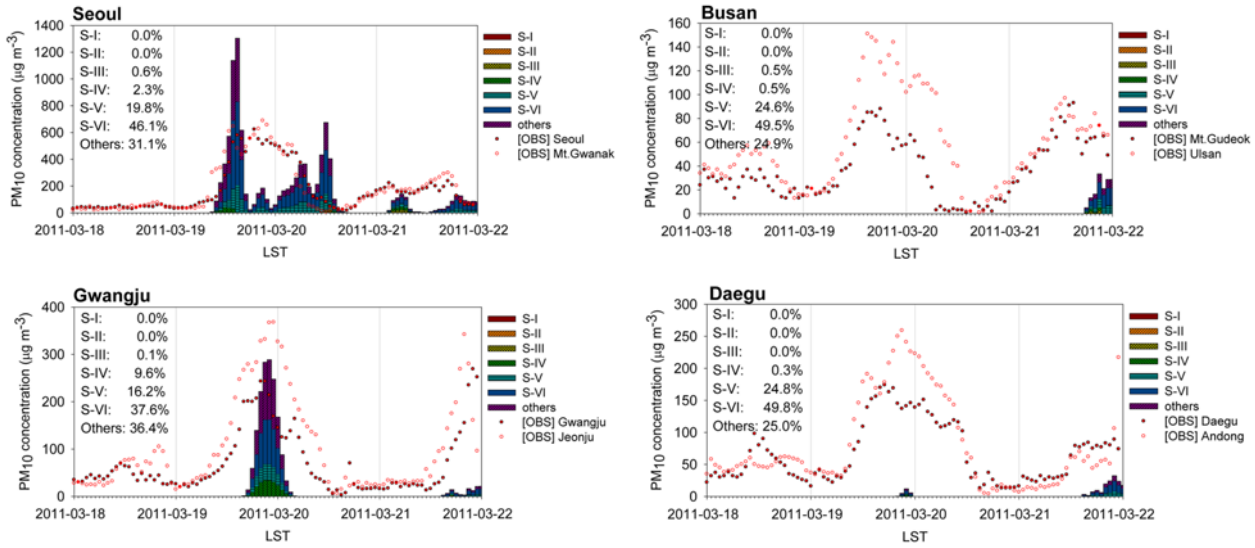


Fig. 8. Comparison of time-series of surface dust concentrations simulated by the LDM against observed surface PM_{10} concentrations for Period A. Simulated source-receptor relationships are also shown here.

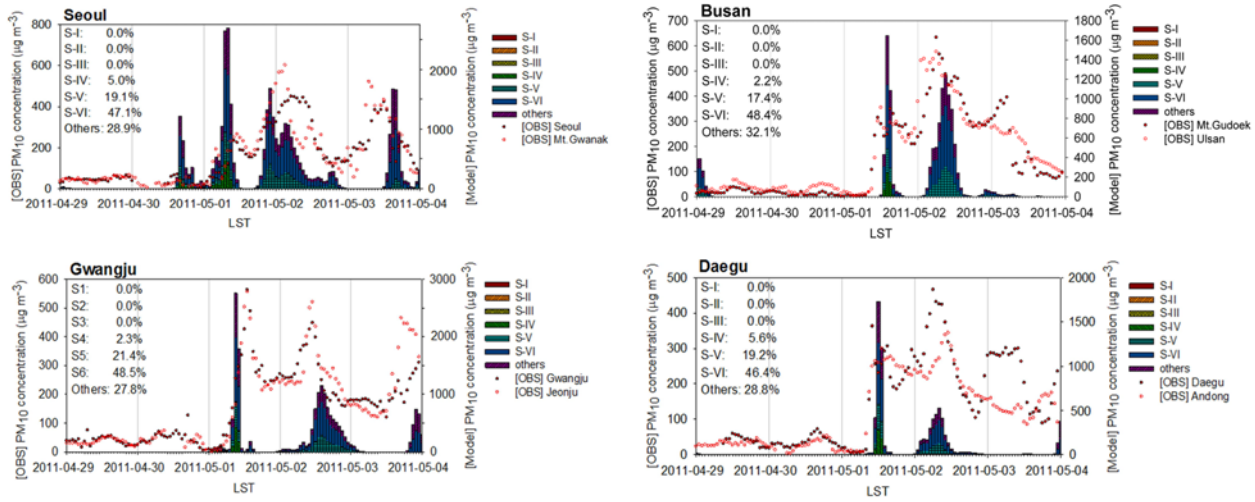


Fig. 9. Comparison of time-series of surface dust concentrations simulated by the LDM against observed surface PM_{10} concentrations for Period B. Simulated source-receptor relationships are also shown here.

of 1,300 μg m^{-3} was higher than the observed maximum value by a factor of two or more, but time variations during Period A were well captured by the model, meaning the model was successful to a certain degree. The model simulated time variations in relatively more sporadic patterns with separate peaks, while observations showed dust event that lasted longer than model events. This is believed to be results of the model systematic error and emission overestimations. It also results from the fact that the observations are originating not only from natural dust mobilization but partly from anthropogenic and secondary aerosol generation processes. Of the six source regions, S-VI contributed to peaks of simulated dust concentrations by up to 46.1%.

In the Gwangju metropolitan area, on March 19, higher dust concentrations were also found at Gwangju and Jeonju sites with the peaks of around 300 μg m^{-3}. The model successfully captured the peak dust concentrations again with S-R relationships of more than 37.6% and 16.2% contributed by S-VI and S-V, respectively. The simulated and measured maximum differ by a factor of less than 1.2, which is not very large, except on March 19 at both sites. It was also promising that the LDM with a horizontal grid of 30 × 30 km cells had the ability to capture peak values. There are secondary peaks observed on March 21-22, 2011; however, the model did not simulate these peaks successfully.

Other sites located in the Busan and Daegu metropolitan areas also showed measured peaks of around 100-200 μg m^{-3} on March 19-20, and secondary peaks of 80-100 μg m^{-3} on March 21-22. However, no PM_{10} concentrations were simulated by LDM (Fig. 8), which is believed to be responsible for the inappropriate transport process simulated by the mesoscale wind fields. This finding confirms that a good mesoscale meteorological model is necessary for dust transport simulations.

For Period B, the LDM successfully captured the timing of dust peaks at all sites to a certain degree. In the Seoul, Busan, and Daegu metropolitan areas, the simulated results showed primary and secondary peaks on 1-2 May. The observed peaks are all found over the same two days. In Seoul, the first peak was simulated on 1 May with a maximum level of 2,500 μg m^{-3}, contributed by S-IV (5%), S-V (19.1%), and S-VI (47.1%). However, the measured PM_{10} levels in most sites are ~600 μg m^{-3}, showing the model and observations differ by factors of 4 or more.

The values were overestimated for the Gwangju metropolitan area as well. The maximum value of 500 μg m^{-3} was observed on May 1 in the Gwangju metropolitan area, but the model simulated 3,000 μg m^{-3}, which is ~6 times the observed value. However, the model simulated the time of the maximum and the starting time of the dust event very accurately. The S-R relationships of 2.3% (by S-VI), 21.4% (by S-V), and 48.5% (by S-VI) in the Gwangju metropolitan area show contributions similar to those in Seoul metropolitan area.

In the Busan and Daegu metropolitan areas, the primary and secondary peaks are observed on May 1 and 2, and the model also simulated the time of the two peaks reasonably well. However, the model overestimated dust concentrations by a factor of 3-5, as in the case of the other locations. Further model development, including a multi-bin dust size distribution, is expected to improve this failure in the current single-modal model. The S-R relationships in both the Busan and Daegu metropolitan areas showed 2.2-5.6% (by S-IV), 17.4-19.2% (by S-V), and 46.4-48.4% (by S-VI), indicating that S-VI is the main source region in the Korean Peninsula.

Table 4 summarizes the results of statistical parameters (Willmott, 1981; Klung *et al*., 1992) for comparisons between simulations and observations at eight sites located in four metropolitan cities. The observed ensemble average of eight sites for Periods A and B are 75.1 μg m^{-3} and 151.0 μg m^{-3}, respectively. However, the simulated mean values are 25.8 μg m^{-3} and 336.6 μg m^{-3}, showing low model predictions for Period A and high model predictions for Period B. The underestimation for Period A is mainly due to the simulation failure over the Busan and Daegu metropolitan areas, as indicated in Fig. 8. This suggests that more emission estimation tests are needed for various meteorological conditions to achieve robust dust mobilization parameterizations. RMSEs are 99.1~331.4 μg m^{-3} for Periods A and B, respectively, and the average absolute gross error (AGE) equals 59.2 μg m^{-3} and 207.1 μg m^{-3} for the two periods, respectively. This implies a rather high discrepancy for Period B because of the overestimation in the model simulation. The unsystematic error (UMSE) is smaller

Table 4. Summary of statistical comparisons of modeled dust concentrations and observations.

	(Period A)		(Period B)	
	Model	**Observation**	**Model**	**Observation**
Sample size	580	580	580	580
Range (μg·m^{-3})	~1305	1~ 623	~2860	10.2~ 389.5
Mean (μg·m^{-3})	25.8	68.7	336.6	151.0
Standard Deviation (SD)(μg·m^{-3})	98.4	91.7	256.5	135.6

	(Period A)	**(Period B)**
Normalized mean difference (NMD)	0.6	-1.5
Root Mean Square Error (RMSE)	99.1	331.4
Average absolute gross error (AGE)	59.2	207.1
Index of agreement (IOA)	0.8	0.4
Unsystematic mean square error (UMSE)	81.5	285.6
Systematic mean square error (SMSE)	56.4	168.0
RMSR $(UMSE^2 + SMSE^2)^{1/2}$	99.1	331.4
Correlation coefficient	0.6	0.5

than the systematic error (SMSE) (Table 4), indicating that the model performance would be more reliable if we employ more precise dust emission data, in addition to other input data, rather than resolving intrinsic uncertainties in the LDM. The indices of agreement also suggest that the results are reasonable for Period A (IOA = 0.8), but Period B shows poor agreement (IOA = 0.4), suggesting the need for further sensitivity tests applied to multiple Asian dust cases.

e. Comparison against Eulerian model ADAM2

Figures 10-11 show the spatial patterns of the daily averaged surface dust concentrations compared with estimates from the Eulerian model ADAM2, for both periods. The simulated dust particles are converted to an Eulerian grid concentration using the simple uniform kernel method described in Section 2.1. As in Figs. 10-11, the results demonstrated similarities between the two models for both periods. However, in spite of the similarities, each model showed differences in simulated dust quantities. The LDM simulated relatively lower concentrations of dust than ADAM2 over the entire duration of Periods A and B. For Period A, the LDM had a domain average of 11.2 μg m^{-3} and ADAM2 had a domain average and 13.6 μg m^{-3}. For Period B, the LDM had a domain average of and 13.1 μg m^{-3}, while ADAM2 had 14.7 μg m^{-3}. This indicates that ADAM2 yielded ~10% higher dust concentrations than the LDM. This

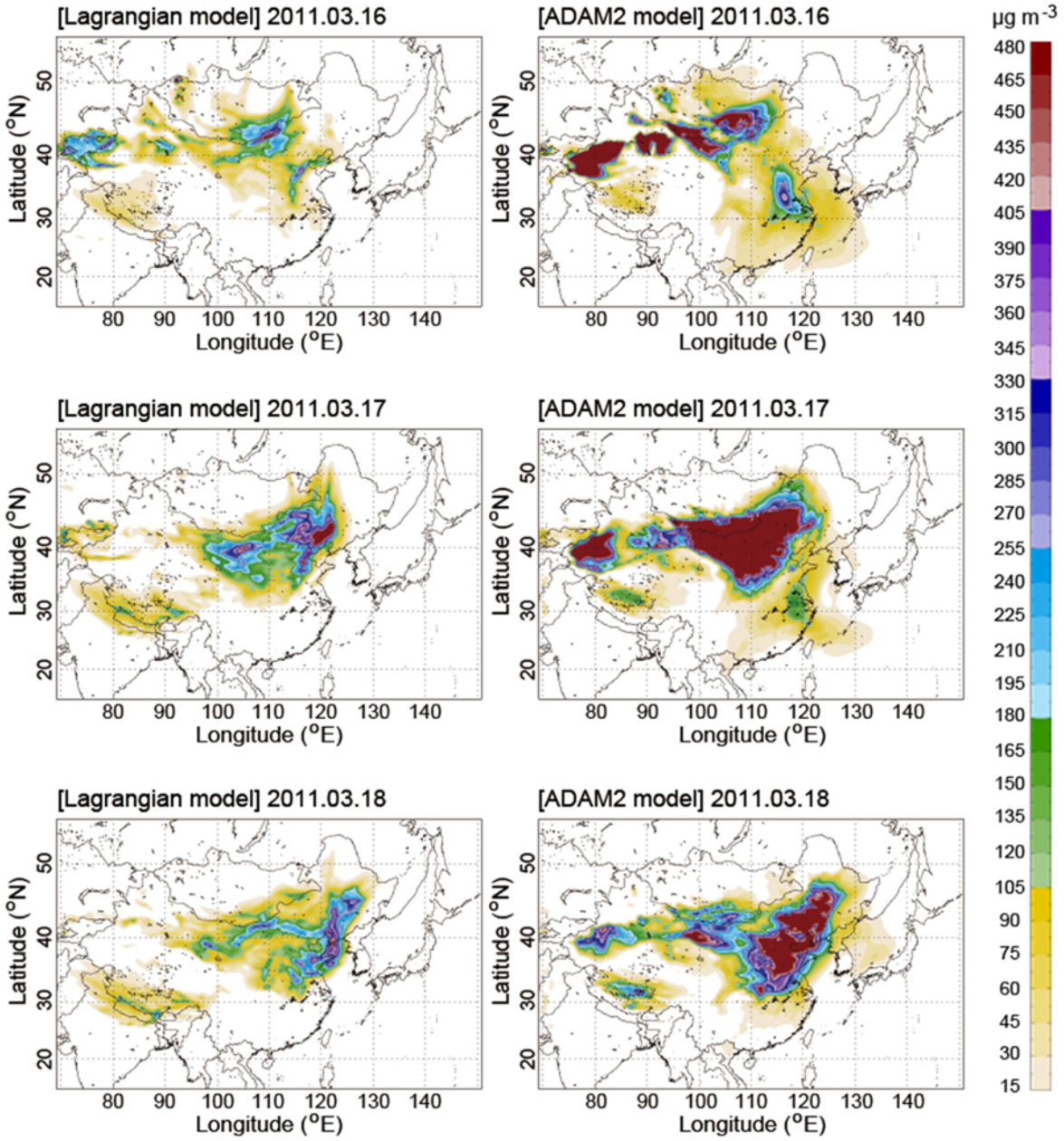


Fig. 10. Comparison of results of the LDM with those of the Eulerian Asian Dust forecasting model, ADAM2, for Period A.

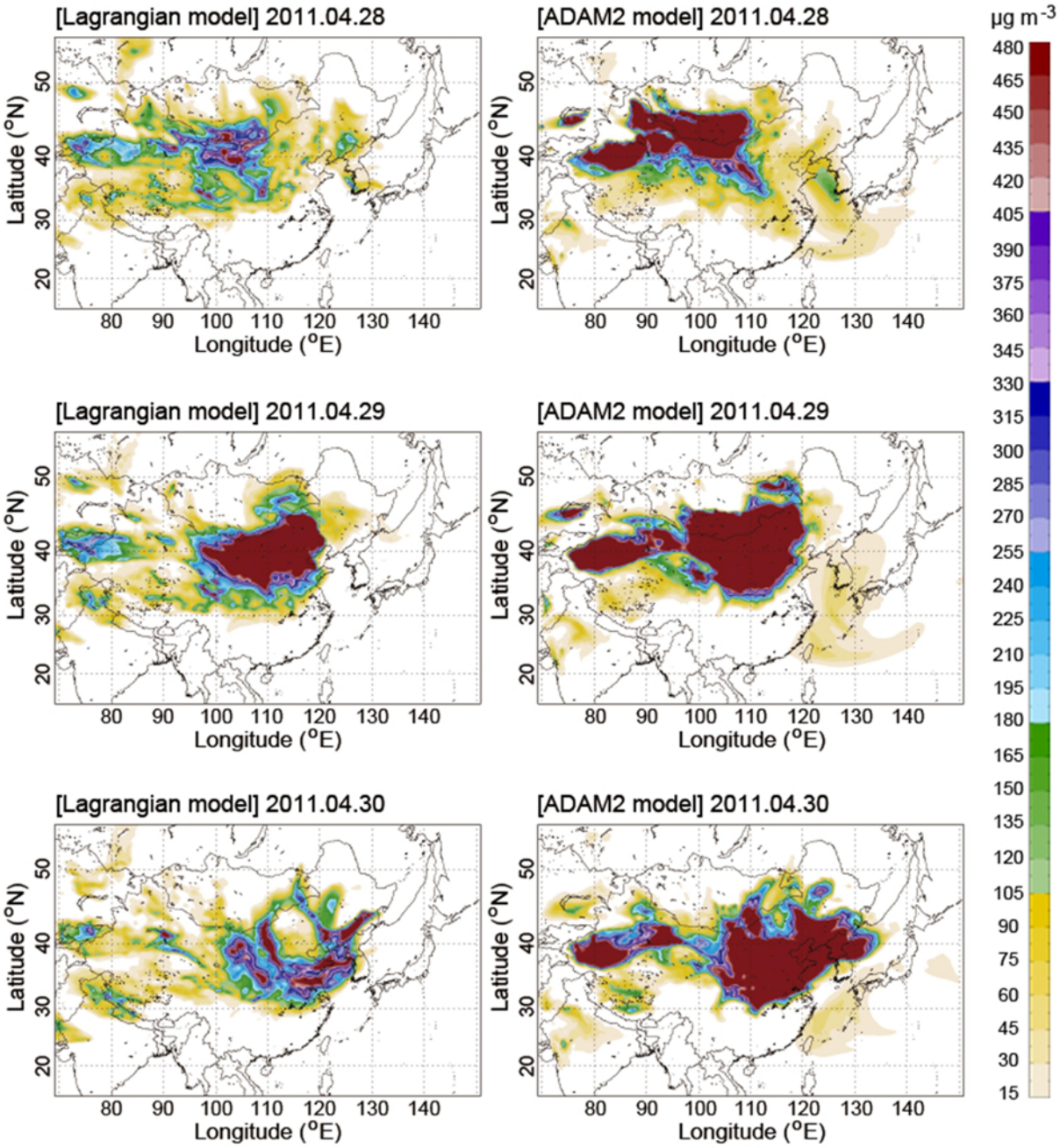


Fig. 11. Comparison of results of the LDM with those of the Eulerian Asian Dust forecasting model, ADAM2, for Period B.

is more apparent on days of higher dust concentrations in Korea. The LDM simulated a maximum concentration of 1,300 μg m^{-3} (Seoul, March 19) for Period A, whereas ADAM2 simulated a maximum concentration of 1,500 μg m^{-3}. This indicates that ADAM2 yielded a dust concentration consistently over 10% higher than the LDM, with a wider region of higher dust concentration (Fig. 10).

These differences are mainly caused by the varying removal processes. The dry and wet deposition in ADAM2 was developed to depend on size distributions, while the LDM employed uni-modal dust removal function was developed without a size dependency. Belly (1964) suggested that the threshold velocity in the dust emission module should take into account the particle size and soil moisture content. Iversen and White (1982), and Greeley and Iversen (1985) parameterized the size dependence of the threshold wind friction velocity, showing that deposition processes are strongly sensitive to the size distributions.

Another possible cause is the difference of dry deposition parameterization over the remote and marine atmosphere. In Figs. 10-11, dust concentrations are shown over the Yellow Sea and the East Sea; significantly lower concentrations were

Table 5. Statistical summary of the simulated dust concentrations simulated by LDM and ADAM2 for Periods A and B.

Statistics	Period A	Period B
Root Mean Square Error (RMSE)	91.28	187.20
Pattern Correlation (PC)	0.79	0.83
Absolute Gross Error (AGE)	24.22	47.40
Index of Agreement (IOA)	0.64	0.69

simulated by LDM, causing big differences between two models. In general, the dry deposition velocity was reported to vary according to the effects of dense vegetation (or ocean surface) as described by Wesely's parameterization (Wesely 1989; Walmsley and Wesely, 1996). Our simulations adopted the removal modules of the FLEXPART model (see Appendix B) over the ocean surface. Therefore more detailed sensitivity tests are required to assess the differences in removal processes.

The dust concentrations simulated by the two models are statistically compared. In order to calculate the similarity of the spatial and temporal distribution between two models, a pattern correlation (PC) between the variables A and B was defined as follows,

$$\mathrm{PC} = \frac{\sum(A_i-\overline{A})(B_i-\overline{B})}{[\sum(A_i-\overline{A})^2(B_i-\overline{B})^2]^{1/2}}$$

where N is the number of pairs of the variables A_i and B_i, and $\overline{A_i} = \frac{1}{N}\sum_1^N A_i$ and $\overline{B_i} = \frac{1}{N}\sum_1^N B_i$ are space averaged values. Table 5 summarizes the simulated dust concentrations by the LDM in comparison with ADAM2. Inconsiderable but detectable differences were found between the two models (Fig. 6). A high pattern correlation (PC = 0.79 – 0.83) suggested the plausible results of the dust simulations based on the two simple case studies with the identical input data assumptions. During each period, similarities between models are found, with no significant biases and low RMSE. In addition, an IOA greater than 0.5, the level of good grades discussed in previous studies (Hurley *et al*., 2002), suggests the predictability of the LDM is strong. These low errors between the two models and the high IOAs suggest that the Lagrangian model, LDM, may be effective in quantitative estimations of dust concentrations for severe Asian dust events.

In a Lagrangian frame, the S-R relationship is generally able to explain the contributions to transported dust concentrations. In an Eulerian frame, several simulations with different emission rates from various source regions are needed to calculate the S-R relationship. However, the S-R relationship can be easily computed with the Lagrangian model, LDM, and it can be used effectively, as in the current study, to estimate quantitative source identifications.

5. Conclusions

We developed an uni-modal Lagrangian dust model (LDM) that was used to simulate Asian dust events recently recorded over the Korean Peninsula. The selected dust simulation periods are March 15-22, 2011 (8 days), and April 27-May 4, 2011 (8 days), during which more than 1,000 μg m^{-3} of PM_{10} concentrations are observed in Seoul. ADAM2 (Asian Dust Aerosol Model 2) was employed to estimate dust mobilization and WFR (Weather Research and Forecasting) was used to generate meteorological fields. The simulated dust concentrations are compared with both point measurements and an Eulerian model, ADMA2.

The results showed that the LDM simulated the arriving time of the dust events to the Korean Peninsula very well for both periods, however, the model tended to overestimate dust concentration with a rather high root mean square error and absolute gross error. For some sites, the model did not simulate dust concentration at all (e.g., period A), implying that a good meteorology model is necessary before simulation or forecasting work. However, comparing the LDM simulations with the Eulerian ADAM2, good pattern correlation (PC = 0.78 – 0.83) and high index of agreement (IOA > 0.6) were found. This suggests the possibility of dust concentrations simulation and analysis models with the S-R relationships.

Finally, additional model sensitivity tests are critical to making improvements on dust simulation and assessing transport process in the target region. This requires more theoretical research, additional detailed observations, and further improvements in the model. Additional model sensitivity tests, including examining the size dependent wet and dry removal process in association with dust prediction, will be considered, and an intensive monitoring and data assimilation process are necessary to improve the prediction of the Asian dust events.

Acknowledgments. This subject is supported by Korea Ministry of Environment as "Climate Change Correspondence R&D Program", and also supported by Basic Science Research Program through the National Research Foundation of Korea (NRF) funded by the Ministry of Education, Science and Technology (2010-0022134).

Edited by: Rokjin Park

Appendix 1. Parameterization of the wind fluctuations

For standard deviation of turbulent wind components, σ_{vi} (σ_u, σ_v, σ_w) and Lagrangian integral timescale T_{Li} (T_{Lu}, T_{Lv}, T_{Lw}) were proposed by Hanna (1982), and parameterizations are expressed based on the boundary layer parameters variables such as h, L, w_*, z_0 and u_*. Here h, L, w_*, z_0, f, and u_* represent ABL height, Monin-Obukhov length, convective velocity scale, roughness length, Coriolis parameter, and friction velocity, respectively. A modification was taken from Ryall *et al*. (1997) for σ_w as follows:

Unstable conditions

$$\frac{\sigma_u}{u_*} = \frac{\sigma_v}{u_*} = \left(12 + \frac{h}{2|L|}\right)^{0.3}$$

$$T_{Lu} = T_{Lv} = 0.15\frac{h}{\sigma_u}$$

$$\sigma_w = [1.2\, w_*^2\,(1 - 0.9\frac{z}{h})\,(\frac{z}{h})^{2/3} + (1.8 - 1.4\frac{z}{h})u_*^2]^{1/2}$$

For $\frac{z}{h} < 0.1$ and $z - z_o > -L$:

$$T_{Lw} = 0.1\frac{z}{\sigma_w[0.55 - 0.38(z - z_0)/L]}$$

For $\frac{z}{h} < 0.1$ and $z - z_o < -L$:

$$T_{Lw} = 0.59\frac{z}{\sigma_w}$$

For $\frac{z}{h} > 0.1$:

$$T_{Lw} = 0.15\left(\frac{h}{\sigma_w}\right)\left[1 - \exp\left(\frac{-5z}{h}\right)\right]$$

Neutral conditions:

$$\frac{\sigma_u}{u_*} = 2.0\,\exp(-3fz/u_*)$$

$$\frac{\sigma_v}{u_*} = \frac{\sigma_w}{u_*} = 1.3\,\exp(-2fz/u_*)$$

$$T_{Lu} = T_{Lv} = T_{Lv} = \frac{0.5z/\sigma_w}{1 + 15fz/u_*}$$

Stable conditions:

$$\frac{\sigma_u}{u_*} = 2.0\,(1 - \frac{z}{h})$$

$$\frac{\sigma_v}{u_*} = \frac{\sigma_w}{u_*} = 1.3\,(1 - \frac{z}{h})$$

$$T_{Lu} = 0.15\,v_g$$

$$T_{Lv} = 0.07\left(\frac{h}{\sigma_v}\right)\left(\frac{z}{h}\right)^{0.5}$$

$$T_{Lw} = 0.1\left(\frac{h}{\sigma_w}\right)\left(\frac{z}{h}\right)^{0.5}$$

Lacking suitable turbulence parameterizations above the ABL ($z > h$), a constant vertical diffusivity $D_z = 0.1\ m^2\,s^{-1}$ is used in the stratosphere, following recent work of Legras *et al.* (2003), whereas a horizontal diffusivity $D_h = 50\ m^2\,s^{-1}$ is used in the free troposphere. Stratosphere and troposphere are distinguished based on a threshold of 2 pvu (potential vorticity units). Diffusivities are converted into velocity scales using $\sigma_{vi} = \sqrt{D_i/dt}$.

Appendix 2.

2-1. Dry deposition

Dry deposition is described by a deposition velocity

$$v_d(z) = -F_C/C(z)$$

where F_C and C are the flux and the concentration of a species at height z within the constant flux layer. Dry deposition velocity of particles, $v_d(z)$ can be described by

$$v_d(z) = [r_a(z) + r_b + r_a(z)\cdot r_b\cdot v_g]^{-1} + v_g$$

where v_g is the gravitational settling velocity calculated from (Slinn, 1982)

$$v_g = \frac{g\rho_p d_p^2 C_{cun}}{18\mu}$$

where ρ_p and dp are the particle density and diameter, μ the dynamic viscosity of air ($0.000018\ kg\,m^{-1}\,s^{-1}$) and C_{cun} the Cunningham slip-flow correction.

Settling and dry deposition velocities are strongly dependent on particulate size. LDM assumes a logarithmic normal size distribution of the particulate mass. The user must specify the mean particulate diameter $\overline{d_p}$ and a measure of the variation around $\overline{d_p}$, σ_p. Then, the settling and deposition velocities are calculated for several particle diameters and are weighted with their respective particulate mass fractions. Gravitational settling is important not only for the computation of the dry deposition velocity, but also affects the particle's trajectory. As a particle can normally represent several species, gravitational settling can only be taken into account correctly (i.e., influence particle trajectories) in single-species simulations.

2-2. Wet deposition

In-cloud and below-cloud scavenging are treated differently. Based on the humidity and temperature from the meteorological input data, the occurrence of clouds is calculated. If relative humidity exceeds 80% the occurrence of a cloud is assumed.

In cloud scavenging is treated differently for gases and particles. The implementation follows the scheme of Hertel *et al.* (1995). In general, the scavenging coefficient $\Lambda(s^{-1})$ depends on the precipitation rate I (mm h^{-1}) and the height H_i over which scavenging takes place:

$$\Lambda = \frac{S_i I}{H_i}$$

S_i is different for gases and particles. For particles, Si = 0.9/cl. where *cl* is the cloud liquid water content

$$cl = 2 \times 10^{-7}\cdot I^{0.36}$$

Below cloud scavenging takes the form of an exponential decay process (McMahon, 1979). With the scavenging coefficient Λ, wet deposition is described as

$$m(t + \Delta t) = m(t)\ exp(-\Lambda\Delta t)$$

where m is the particle mass. Λ increases with the precipitation rate I according to

$$\Lambda = AI^B$$

where A [s^{-1}] is the scavenging coefficient at I = 1 mm/hour and B gives the dependency on precipitation rate. Both A and B must be specified but LDM uses the same scavenging coefficients for snow and rain. As wet deposition depends nonlinearly on precipitation rate, subgrid variability of precipitation must be accounted for (Hertel *et al*., 1995). The area fraction which experiences precipitation given a certain grid-scale precipitation rate is calculated by

$$F = \max\left[0.05, CC\frac{I_l fr_l(I_l) + I_c fr_c(I_c)}{I_l + I_c}\right]$$

Table 6. Correction factors used for the calculation of the area fraction that experiences precipitation. Precipitation rates are in mm $hour^{-1}$.

	I_l and I_c				
Factor	I ≤ 1	1 < I ≤ 3	3 < I ≤ 8	8 < I ≤ 20	20 < I
fr_l	0.50	0.65	0.80	0.90	0.95
fr_c	0.40	0.55	0.70	0.80	0.90

where CC is the total cloud cover, I_l and I_c are the large scale and convective precipitation rates, respectively, and fr_l and fr_c are correction factors that depend on I_l and I_c (see Table 6). The subgrid scale precipitation rate is then $I_s = (I_l + I_c)/F$.

REFERENCES

Asman, W. A. H., 1995: Parameterization of below-cloud scavenging of highly soluble gases under convective conditions. *Atmos. Environ.*, **29**, 1359-1368.

Batsukh, S., 2004: Geographic Atlas of Mongolia. Administration of Land Affairs. Geodesy and Cartography, Ulaanbaatar, 62 pp.

Belly, P.Y., 1964: Sand movement by wind, U.S. Army Coastal Eng. Res. Tech. Memo.

Buritt, B., and A. D. Hyers, 1981: Evaluation of Arizona's highway dust warning system. *Geolog. Soc. of America Bulletin Special Paper*, **186**, 282-292.

Chock, D. P., and S. L. Winkler, 1994: A particle grid air quality modeling approach 1. The dispersion aspect. *J. Geophys. Res.*, **99**, 1019-1031.

Collins, J., D. S. Stevenson, C. E. Johnson, and R. G. Derwent, 1997: Tropospheric ozone in a global-scale three-dimensional Lagrangian model and its response to NOx emission controls. *J. Atmos. Chem.*, **26**, 223-274.

Dabdub, D., and J. H. Seinfeld, 1994: Numerical advective schemes used in air quality models sequential and parallel implementation. *Atmos. Environ.*, **28**, 3369-3385.

Gillette, D. A., J. Adams, A. Endo, and D. Smith, 1980: Threshold velocities for input of soil particles in the air by desert soils. *J. Geophys. Res.*, **85**, 5621- 5630.

_____, _____, D. Muhs, and R. Kihl, 1982: Threshold velocities and rupture moduli for crusted desert soils for the input of soil particles into the air. *J. Geophys. Res.*, **87**, 9003-9015.

Gong, S. L., X. Y. Zhang, T. L. Zhao, I. G. McKendry, D. A. Jaffe, and N. M. Lu, 2003: Characterization of soil dust aerosol in China and its transport and distribution during 2001 ACE-Asia: 2. Model simulation and validation. *J. Geophys. Res*., **108(D9)**, 4262, doi:10.1029/2002-JD002633.

Goudie, A. S., 1977: Sodium sulphate weathering and the disintegration of Mohenjo Daro, Pakistan. Earth Surface Process 2, 75-86.

Greeley, R., and Iversen, J. D., 1985: *Wind as a Geological Process on Earth, Mars, Venus and Titan.* Cambridge University Press, New York.

Hagen, L., and N. O. Woodruff, 1973: Air pollution in the Great Plains. *Atmos. Environ.*, **7**, 323-332.

Hanna, S. R., 1982: Applications in air pollution modeling. In: Nieuwstadt F.T.M. and H. van Dop (ed.): Atmospheric Turbulence and Air Pollution Modelling. D. Reidel Publishing Company, Dordrecht, Holland, 1982.

Harrison, S. P., K. E. Kohfeld, C. Roelandt, and T. Claquin, 2011: The role of dust in climate changes today, at the last glacial maximum and in the future. *Earth-Science Reviews*, **54(1-3)**, 43-80.

Haywood, J., and O. Boucher, 2000: Estimates of the direct and indirect radiative forcing due to tropospheric aerosols: A review. *Rev. Geophys.*, **38**, 513-543.

Helgren, D. A., and J. M. Prospero, 1987: Wind velocities associated with dust deflation events in the western Sahara. *J. Climate Appl. Meteor.*, **26**, 1147- 1151.

Hertel, O., J. Christensen, E. H. Runge, W. A. H. Asman, R. Berkowicz, M. F. Hovmand, and O. Hov, 1995: Development and testing of a new variable scale air pollution model - ACDEP. *Atmos. Environ.*, **29**, 1267-1290.

Hurley P. J, L. P. William, and K. L. Ashok, 2002: The Air Pollution Model (TAPM) version 2: summary of some verification studies. CSIRO, Clayton.

In, H.-J., and S.-U. Park, 2002: A simulation of long-range transport of Yellow Sand observed in April 1998 in Korea. *Atmos. Environ.*, **36**, 4173-4187.

_____, and _____, 2003: A simulation of long-range transport of yellow sand observed in April 1998 in Korea. *Atmos. Environ.*, **36**, 4625- 4636.

Iversen, J. D., and B. R. White, 1982: Saltation threshold on Earth, Mars and Venus. *Sedimentology*, **29**, 111-119.

Kalma, J. D., J. G. Speight, and R. J. Ludwig, 1988: Potential wind erosion in Australia: A continental perspective. *J. Climatol.,* **8**, 411-428.

Klemp, J. B., W. C. Skamarock, and J. Dudhia, 2000: Conservative split-explicit time integration methods for the compressible nonhydrostatic equations. [Available online at http://wrf-model.org/WG1/wg1pmain.html].

Klung W, G. Graziani, G. Grippa, D. Pierce, and C. Tassone, 1992: The ATMES report. Elsevier, London.

Kurosaki, Y., and M. Mikami, 2003: Recent frequent dust events and their relation to surface wind in East Asia. *Geophys. Res. Lett.,* **30**, 1736.

_____, and _____, 2005: Regional difference in the characteristic of dust event in East Asia: Relationship among dust outbreak, surface wind, and land surface condition. *J. Meteor. Soc. Japan*, **83A**, 1-18.

_____, and _____, 2007: Threshold wind speed for dust emission in east Asia and its seasonal variations. *J. Geophys. Res.,* **112**, D17202.

Legg, B. J., and M. R. Raupach, 1982: Markov-chain simulation of particle dispersion in inhomogeneous flows: the mean drift velocity induced by a gradient in Eulerian velocity variance. *Bound. -Layer Meteor.*, **24**, 3-13.

Legras, B., B. Joseph, and F. Lefevre, 2003: Vertical diffusivity in the lower stratosphere from Lagrangian back-trajectory reconstructions of ozone

profiles. *J. Geophys. Res.*, **108**, 4562, doi:10.1029/2002JD003045.

Lim, J.Y., and Y. S. Chun, 2006: The characteristics of Asian dust events in Northeast Asia during the springtime from 1993 to 2004. *Global Planet. Change*, **52**, 231-247.

Liu, M., D. L. Westphal, S. Wang, A. Shimizu, N. Sugimoto, J. Zhou, and Y. Chen, 2003: A high-resolution numerical study of the Asian dust storms of April 2001. *J. Geophys. Res.*, **108(D23)**, 8653, doi:10.1029/2002JD003178.

McMahon, T. A., and P. J. Denison, 1979: Empirical atmospheric deposition parameters - a survey. *Atmos. Environ.*, **13**, 571-585.

Park, S.-U., and H.-J. In, 2003: Parameterization of dust emission for the simulation of the yellow sand (Asian dust) event observed in March 2002 in Korea. *J. Geophys. Res.,* **108**, 4618.

_____, and E.-H. Lee, 2004: Parameterization of Asian dust (Hwangsa) particle-size distributions for use in dust emission models. *Atmos. Environ.*, **38**, 2155-2162.

Peters, L. K., and Coauthors, 1995: The current state and future direction of Eulerian models in simulating the tropospheric chemistry and transport of trace species-a review. *Atmos. Environ.*, **29**, 189-222.

Russell, A., and R. Dennis, 2000: NARSTO critical review of photochemical models and modeling. *Atmos. Environ.*, **34**, 2283-2324.

Ryall, D. B. and R. H. Maryon, 1997: Validation of the UK Met Office's NAME model against the ETEX dataset. In: Nodop, K. (editor): ETEX Symposium on Long-Range Atmospheric Transport, Model Verification and Emergency Response, European Commission EUR 17346, 151-154.

Shao, Y., and Coauthors, 2003: Northeast Asian dust storms: Real-time numerical prediction and validation. *J. Geophys. Res.,* **108**, 1-18.

Slinn, W. G. N., 1982: Predictions for particle deposition to vegetative canopies. *Atmos. Environ.*, **16**, 1785-1794.

Stohl, A., 1998: Computation, accuracy and applications of trajectory - a review and bibliography. *Atmos. Environ.,* **32**, 947-966.

_____, C. Forster, A. Frank, P. Seibert, and G. Wotawa, 2005: Technical note: The Lagrangian particle dispersion model FLEXPART version 6.2., *Atmos. Chem. Phys.*, **5**, 2461-2474.

Tegen, I., and I. Fung, 1994: Modeling of mineral dust in the atmosphere: Sources, transport, and optical thickness. *J. Geophys. Res.*, **99**, 22897-22914.

Thomson D. J., 1987: Criteria for the selection of stochastic models of particle trajectories in turbulent flows. *J. Fluid Mech.*, **180**, 529-556.

Uno, I., H. Amano, S. Emori, K. Kinoshita, I. Matsui, and N. Sugimoto, 2001: Trans-Pacific yellow sand transport observed in April 1998: A numerical simulation. *J. Geophys. Res.*, **106**, 18,331-18,344.

_____, and Coauthors, 2003: Regional chemical weather forecasting system CFORS: model descriptions and analysis of surface observations at Japanese island stations during the ACE-Asia experiment. *J. Geophys. Res.*, **108**, 8668.

Walmsley, J. L, and M. L.Wesely, 1996: Modification of coded parameterizations of surface resistances to gaseous dry deposition. *Atmos. Environ.,* **30**, 1181-1188.

Wang, Z., H. Ueda, and M. Huang, 2000: A deflation module for use in modeling long-range transport of yellow sand over East Asia. *J. Geophys. Res.*, **105**, 26,947- 26,960.

Wang, X., Y. Yang, Z. Dong, and C. Zhang, 2009: Responses of dune activity and desertification in China to global warming in thetwenty-first century. *Global Planet. Change*, **67**, 167-185.

Wesely, M. L., and B. B. Hicks, 1977: Some factors that affect the deposition rates of sulfur dioxide and similar gases on vegetation. *J. Air Pollut. Control Assoc*., **27**, 1110-1116.

_____, 1989: Parameterization of surface resistances to gaseous dry deposition in regional-scale numerical models. *Atmos. Environ.*, **23**, 1293-1304.

Westphal, D. L., O. B. Toon, and T. N. Carlson, 1988: A case study of mobilization and transport of Saharan dust. *J. Atmos. Sci.*, **45**, 2145-2175.

Willmott, C. J., 1981: On the validation of models. *Phys Geogr.,* **2**, 184-194.

Xu, Z, Y. Li, Y. Tang, and G. Han, 2009: Chemical and strontium isotope characterization of rainwater at an urban site in Loess Plateau, Northwest China. *Atmos. Res*., **94**, 481-490.

Yang, S., and Z. Ding, 2008: Advance-retreat history of the East-Asian summer monsoon rainfall belt over northern China during the last two glacial-interglacial cycles. *Earth Planet. Sci. Lett.*, **274**, 499-510.